

A detailed chemical kinetics model for the combustion of gas-phase guanidine nitrate

Yu-ichiro Izato^{*,**†} and Atsumi Miyake^{**}

*Graduate School of Environment and Information Sciences, Yokohama National University, 79-7 Tokiwadai, Hodogaya-ku, Yokohama-shi, Kanagawa, 240-8501 JAPAN

Phone: +81-45-339-3981

†Corresponding author: izato-yuichiro-hk@ynu.jp

**Institute of Advanced Sciences, Yokohama National University, 79-5 Tokiwadai, Hodogaya-ku, Yokohama-shi, Kanagawa, 240-8501 JAPAN

Received: July 21, 2017 Accepted: August 10, 2018

Abstract

The combustion mechanism of guanidine nitrate (GN) in the gas phase was investigated, and a detailed chemical kinetics model based on quantum chemical calculations was developed. 39 reactions associated with GN combustion were identified and added to our previous model. Optimized structures of reactants, products, and transition states were obtained at the ω B97X-D/6-311++G(d,p) level of theory and the total electron energies of such structures were calculated at the CBS-QB3 level of theory. Transition state theory was used to calculate the kinetics parameters from the quantum chemistry calculations. Detailed chemical reaction calculations revealed the combustion behavior and mechanism of a GN and basic copper (II) nitrate (BCN) mixture. At the initial temperature of 1173 K, the GN/BCN mixture has four zones in the flame structure: the first ignition, the first flame, the second ignition, and the second flame. The combustion reaction is triggered by the HNO_3 decomposition to $\text{OH}\cdot$ and $\text{NO}_2\cdot$, and the radicals attack CN_3H_5 (the first ignition). Remaining CH_5N_3 is consumed by self-decomposition: $\text{CH}_5\text{N}_3 \rightarrow \text{NH}_3 + \text{HNCNH}$ (the first flame) and then HNCNH , NH_3 and NO_x gas burn out (in the second ignition and flame).

Keywords: guanidine nitrate, gas-generation agent, combustion, kinetic model, *ab initio* calculation

1. Introduction

Energetic compositions release large amounts of gaseous products with exothermic heat in a short time and they have been widely used as propellants, fireworks, blasting agents, or gas generants. Gas generants for car-airbag systems must evolve a large amount of clean gas (low toxicity and environmental friendly). Clean exhausted gas can prevent a driver and fellow passengers from acute poisoning when a car-airbag expands with evolved gas. The amount of heat generated from the combustion must also be small because the low temperature condition allows the use of a plastic sheet as the bag material. In general, plastic sheets cannot withstand high temperatures but they are extremely effective for reducing the weight of the car, leading to good mileage. The use of plastic materials for car airbags is strongly demanded by the auto industry. Thus, the development

and improvement of green propellants that evolve clean exhausted gas and have a small heat of combustion are required.

Guanidine nitrate (GN) is an excellent fuel for a gas-generator propellant. For example, mixtures of GN as the fuel and basic copper nitrate (BCN, $\text{Cu}_2(\text{OH})_3(\text{NO}_3)$) as an oxidizer are well-known as current gas-generating agents and they have been widely applied to car-airbag systems. To improve the combustion properties of GN-based gas generants, many researchers have experimentally studied the decomposition mechanism and the effect of various additives on decomposition^{1)–8)}.

It is necessary to more fully understand the combustion mechanism in order to develop cleaner evolved gas and lower combustion temperature. To this end, combustion simulations based on a detailed chemical kinetic model are effective. Such simulations including detailed kinetic

information can provide deep insight on chemical reactions in a flame and suggest which reactions are key to decreasing harmful gases. Various reliable models for gas-phase reactions associated with energetic materials have been proposed to date, all of which work to explain observed combustion behaviors^{9)–16)}. However, to the best of our knowledge, there are no detailed reaction models for GN combustion.

The purposes of this paper are: (i) to improve the current detailed chemical model by identifying new reactions and providing kinetic data; and (ii) to simulate combustion behavior to gain a better understanding of the combustion mechanism of gaseous GN.

2. Computational

The rate coefficient, k_{TST} , of the generic reaction $A + B \rightarrow$ (products in solution) can be calculated based on traditional transition state theory (TST) using the formula $k_{\text{TST}} = k_{\text{B}}T/h \cdot Q_{\text{TS}}/\Pi Q_{\text{react}} \cdot \exp(-\Delta E_0/RT)$, where k_{B} is Boltzmann's constant, T is temperature, h is Planck's constant, Q_i is the partition function of the reactant and transition state (TS), ΔE is the energy barrier to activation, and R is the universal gas constant. Quantum chemistry calculations were performed to obtain Q_i and ΔE .

The geometries and frequencies of the reactants, products, and transition states were optimized at the $\omega\text{B97X-D}/6\text{-311++G(d,p)}$ level¹⁷⁾ of theory using the Gaussian 09 program package¹⁸⁾. Gordon et al.¹⁷⁾ developed the $\omega\text{B97X-D}$ method, which includes empirical dispersion forces and is believed to be reliable when applied to systems with weak van der Waals forces. Their group also reported that the $\omega\text{B97X-D}$ method yields satisfactory accuracy for kinetics and non-covalent interactions. During computations, transition states (TSs) were extensively searched for and, if found, an intrinsic reaction coordinate (IRC) calculation was conducted in order to assign reactants and products to the TS.

The energies of corresponding molecules were evaluated at the CBS-QB3¹⁹⁾ level of theory, since this is a reasonable time-expense complete basis method. In this study, geometries and frequencies were calculated at the $\omega\text{B97X-D}/6\text{-311++G(d,p)}$ level, the optimized geometries were fixed with no changes allowed and the energies were calculated using the CBS-QB3 method. CBS-QB3 is understood to represent cost-effective strategies for obtaining chemically accurate thermochemical calculations. In this study, geometries and frequencies were calculated at the $\omega\text{B97X-D}/6\text{-311++G(d,p)}$ level of theory, the optimized geometries were fixed with no changes allowed, and the potential energies were calculated using the CBS-QB3 method. In the original CBS-QB3, CBS-Q energy calculations are combined with B3LYP/CBSB7-optimized geometries and frequencies. The five-step series of calculations starts with a geometry optimization at the B3LYP level, followed by a frequency calculation to obtain thermal corrections, zero-point vibrational energy, and entropic information. The next three calculations are single-point calculations at the

CCSD(T), MP4SDQ, and MP2 levels. The CBS extrapolation then gives final energies. In the CBS-QB3// $\omega\text{B97X-D}$ method herein, the potential energy obtained from CBS-QB3 was corrected for the zero-point energy calculated at the $\omega\text{B97X-D}/6\text{-311++G(d,p)}$ level. The performance of the CBS-QB3// $\omega\text{B97X-D}$ method for various gas-species was assessed and validated in Matsugi and Shiina work²⁰⁾.

Transition state theory calculations were performed to obtain the rate coefficient by using the Gaussian postprocessor (GPOP) program suite developed by Miyoshi²¹⁾. GPOP is a collection of tools for the estimation of thermodynamics and rate coefficients for gas-phase reactions.

Thermodynamic data was also developed based on quantum chemistry calculation using the Gaussian 09 program package¹⁸⁾. Optimization and frequency analysis were conducted using the G4²²⁾ level of theory. Thermal correction, entropy (S) and heat capacity (C_p) values were calculated from the partition function using statistical mechanics theory, employing the GPOP software.²¹⁾ The heats of formation for gas-phase molecules ($\Delta_f H_{\text{gas}}^\circ$) were calculated by the traditional atomization method (ARM-1)²³⁾ combined with the G4 level of theory.

3. Results and discussion

3.1 Reaction mechanism

We modeled the kinetics of the GN reaction to develop the YNU 3.0 model, discussed below, improving on the YNU 1.0 model presented previously^{15),16)}. Chemical kinetics parameters are listed in Tables 1 and 2 showing the reactions added into the YNU 1.0 model. The YNU 1.0 model was designed to analyze the decomposition of hydroxylamine¹⁵⁾ and ammonium nitrate¹⁶⁾ gases. We obtained thermodynamic data for major chemical species from existing databases^{24),25)}. Thermodynamic data that were not found in the databases were calculated. Table 3 shows the heats of formation obtained from the ARM-1 combined with the G4 level of theory and the associated thermodynamic data obtained from the partition function using the statistical mechanics theory. Figure 1 depicts chemical structures of reactants, products and intermediates in GN combustion. The new model consists of 80 species and 445 reactions.

3.2 Kinetics modeling

3.2.1 Decomposition of guanidine

This work identified and investigated a mono-molecular decomposition of guanidine (CN_3H_5), as shown below.



CN_3H_5 isomerizes to INT1 via intramolecular hydrogen transfer. This work has revealed that some species (M) aids the decomposition by assisting this intramolecular hydrogen transfer.

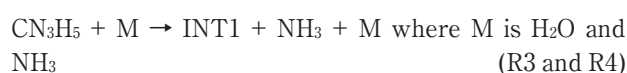


Table 1 Added reactions and rate coefficients employed during the kinetic modeling of GN combustion.

No.	Reaction	ΔH_{298} [kJ mol ⁻¹]		k		
		TS	Product	A^1	n	ΔE_a^2
1	CN ₃ H ₅ ⇌ INT1	203.8	151.1	1.05×10 ⁵	2.26	180.5
2	INT1 ⇌ CHNCH + NH ₃	17.5	-73.2	1.60×10 ¹²	0.58	19.6
3	CN ₃ H ₅ + H ₂ O ⇌ INT1 + H ₂ O	119.7	77.9	1.46×10 ⁻²	3.79	101.0
4	CN ₃ H ₅ + NH ₃ ⇌ INT1 + NH ₃	146.7	77.9	6.98	3.42	83.0
5	CN ₃ H ₅ + HNO ₃ ⇌ HNCNH + NH ₃ + HNO ₃	87.4	77.9	1.25×10 ³	2.62	48.1
6	CN ₃ H ₅ + HONO ⇌ HNCNH + NH ₃ + HONO	109.6	77.9	1.39×10 ¹	3.33	104.2
7	CN ₃ H ₅ + CN ₃ H ₅ ⇌ [CN ₃ H ₅] ₂	66.3	-4.5	6.90	2.97	62.8
8	[CN ₃ H ₅] ₂ ⇌ INT2 + NH ₃	130.4	-11.2	2.08×10 ¹²	0.20	131.9
9	INT2 ⇌ INT3 + NH ₃	280.6	235.6	1.81×10 ¹²	0.57	282.3
10	INT3 ⇌ 2HNCNH	200.6	90.0	2.78×10 ¹⁰	0.81	200.0
11	INT2 + HNO ₃ ⇌ INT3 + NH ₃ + HNO ₃	83.9	81.5	6.90	3.32	79.3
12	CN ₃ H ₅ + OH· ⇌ CN ₃ H ₄ · + H ₂ O	-1.0	-57.2	1.03×10 ³	2.88	-5.5
13	CN ₃ H ₅ + NO ₂ · ⇌ CN ₃ H ₄ · + HONO	90.2	115.3	1.43	3.72	85.8
14	CN ₃ H ₅ + NO ₂ · ⇌ CN ₃ H ₄ · + HNO ₂	91.7	147.6	3.67×10 ⁻¹	3.51	87.2
15	CN ₃ H ₅ + NHCN· ⇌ CN ₃ H ₄ · + HNCNH	45.0	52.4	3.13	3.46	40.7
16	CN ₃ H ₄ · ⇌ NHCN· + NH ₃	236.4	25.5	1.05×10 ⁻⁷	5.62	176.6
17	CN ₃ H ₄ · + H ₂ O ⇌ NHCN· + NH ₃ + H ₂ O	102.5	25.5	9.03×10 ⁻²	3.54	90.2
18	CN ₃ H ₄ · + NH ₃ ⇌ NHCN· + NH ₃ + NH ₃	141.8	25.5	9.87×10 ⁻²	3.68	131.3
19	CN ₃ H ₄ · + HNO ₃ ⇌ NHCN· + NH ₃ + HNO ₃	49.9	25.5	1.25×10 ³	2.62	48.1
20	CN ₃ H ₄ · + HONO ⇌ NHCN· + NH ₃ + HONO	74.3	25.5	5.59×10 ³	2.25	73.6
21	CN ₃ H ₄ · + NO ₂ · ⇌ CN ₃ H ₄ NO ₂	-37.6	-190.6	4.18×10 ¹	3.01	-40.2
22	CN ₃ H ₄ NO ₂ ⇌ HNCNH + <i>trans</i> -NHNO ₂ H	142.3	105.4	3.66×10 ⁷	1.87	136.7
23	<i>trans</i> -NHNO ₂ H ⇌ <i>cis</i> -NHNO ₂ H	110.0	1.5	3.88×10 ¹	3.11	76.0
24	<i>trans</i> -NHNO ₂ H + H ₂ O ⇌ <i>cis</i> -NHNO ₂ H + H ₂ O	9.1	1.5	2.17×10 ⁻¹	3.34	-2.4
25	<i>cis</i> -NHNO ₂ H ⇌ N ₂ O + H ₂ O	130.0	-203.3	6.22×10 ¹⁰	1.03	125.4
26	<i>cis</i> -NHNO ₂ H + H ₂ O ⇌ N ₂ O + 2H ₂ O	45.1	-203.3	9.38×10 ⁻²	3.77	34.4

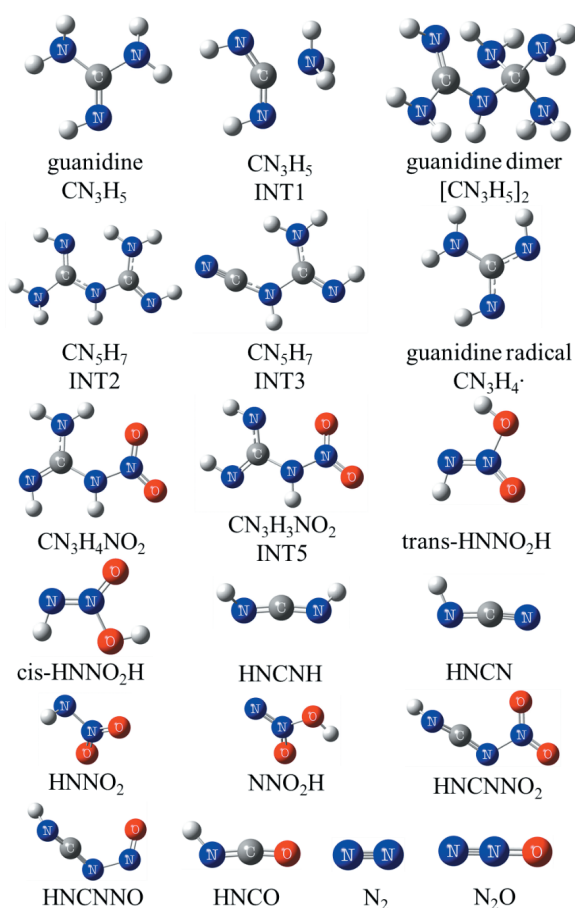
¹ Frequency factor is given in units of [cm³], [mol], and [s].² Activation energy is in units [kJ mol⁻¹].**Table 2** Added reactions and rate coefficients employed during the kinetic modeling of GN combustion (successive).

No.	Reaction	ΔH_{298} [kJ mol ⁻¹]		k		
		TS	Product	A^1	n	ΔE_a^2
27	CN ₃ H ₄ NO ₂ · + OH· ⇌ CN ₃ H ₃ NO ₂ · + H ₂ O	20.0	-44.8	1.09×10 ⁻⁴	4.81	-0.2
28	CN ₃ H ₄ NO ₂ · + NO ₂ · ⇌ CN ₃ H ₃ NO ₂ · + HONO	112.4	127.7	5.12×10 ¹	2.72	110.4
29	CN ₃ H ₄ NO ₂ · + NO ₂ · ⇌ CN ₃ H ₃ NO ₂ · + HNO ₂	137.1	160.0	8.68×10 ¹	2.75	135.0
30	CN ₃ H ₃ NO ₂ · ⇌ HNCNH + HNNO ₂ ·	109.7	58.6	9.16×10 ⁸	1.58	106.3
31	HNNO ₂ · ⇌ NNO ₂ H·	116.2	3.8	4.12	3.35	80.0
32	NNO ₂ H· ⇌ OH· + N ₂ O	12.0	-130.0	4.66×10 ¹²	0.39	12.4
33	HNCNH + OH· ⇌ NHCN· + H ₂ O	7.4	-109.6	1.96×10 ³	2.88	1.7
34	HNCNH + NO ₂ · ⇌ NHCN· + HONO	100.6	62.9	1.59×10 ⁻⁴	4.62	78.1
35	HNCNH + NO ₂ · ⇌ NHCN· + HNO ₂	102.1	95.2	6.00×10 ⁻¹	3.67	79.6
36	NHCN + NO ₂ · ⇌ HNCONO ₂	-12.1	-89.6	1.43×10 ³	2.98	-14.6
37	HNCONO ₂ ⇌ N ₂ O + HNCO	63.8	-302.0	6.25×10 ¹¹	0.15	65.0
38	NHCN· + NO· ⇌ N ₂ + HNCONO	-18.3	-524.5	3.84×10 ²	2.24	-20.3
39	HNCONO ⇌ N ₂ + HNCO	60.2	-302.0	6.63×10 ¹¹	0.15	61.2

¹ Frequency factor is given in units of [cm³], [mol], and [s].² Activation energy is in units [kJ mol⁻¹].

Table 3 Collections of thermodynamic data for GN combustion.

Species	$\Delta_f H^\circ_{calc}$ [kJ mol ⁻¹]	S°_{calc} [J K ⁻¹ mol ⁻¹]	C_p [J K ⁻¹ mol ⁻¹]						
			300 K	400 K	500 K	600 K	800 K	1000 K	1500 K
CN ₃ H ₄ [•]	226.1	291.1	74.1	90.1	102.9	113.0	121.0	127.6	133.3
INT1	179.1	198.4	77.3	94.6	108.9	120.6	138.3	151.4	173.0
[CN ₃ H ₅] ₂	50.1	384.8	158.0	196.8	228.3	253.4	290.7	317.7	361.7
INT2	82.7	355.4	125.1	155.2	179.5	198.9	227.4	247.9	280.7
INT3	206.0	333.4	100.8	120.0	135.2	147.4	165.7	178.9	199.9
HNCNH	147.9	250.2	50.7	59.2	65.2	70.6	74.7	78.0	81.0
NHCN [•]	317.0	311.2	75.2	85.1	92.6	98.5	103.2	107.0	110.2
<i>t</i> -NHNO ₂ H	40.7	273.5	57.0	69.0	78.7	86.4	97.4	105.0	116.3
<i>c</i> -NHNO ₂ H	42.0	274.7	58.5	70.3	79.8	87.3	98.0	105.3	116.4
HNNO ₂	222.1	276.1	50.2	58.3	65.0	70.4	78.0	83.1	90.3
NNO ₂ H	232.0	281.2	57.2	66.2	73.3	78.7	86.3	91.2	98.3
HNCONO ₂	238.9	321.6	81.8	95.9	106.7	114.9	126.4	134.0	144.4
HNCONO	330.7	311.2	75.2	85.1	92.6	98.5	103.2	107.0	110.2

**Figure 1** Chemical structures of reactants, products and intermediates in GN combustion as optimized at the ω B97X-D/6-311++G(d,p) level of theory.

Here, HNO₃ and HONO are more efficient catalysts (M) for CN₃H₅ decomposition due to a one-step conversion to HNCNH and NH₃ with a lower energy barrier.

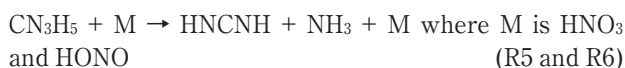
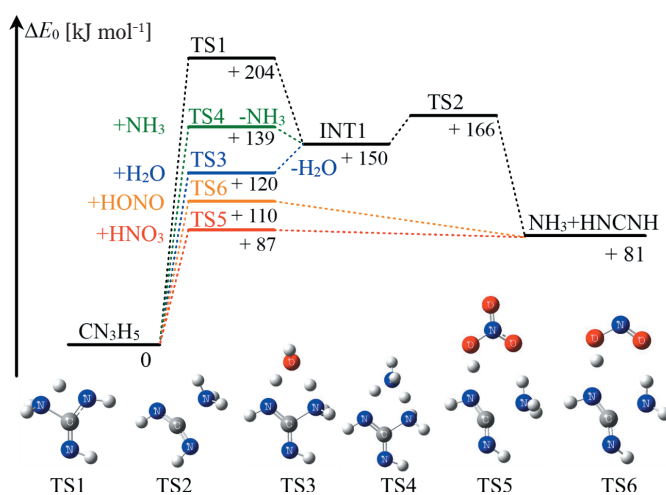


Figure 2 shows the potential energy profiles for the reactions, including the optimized structures of the TSs. The rate coefficients for the reactions were evaluated by

**Figure 2** Potential energy profiles for the decomposition of guanidine. The energy profiles were calculated at the CBS-QB3// ω B97X-D/6-311++G(d,p) level of theory.

simple TST and are listed in Table 1.

This work also identified and investigated a bimolecular decomposition of guanidine (CN₃H₅), as shown below.

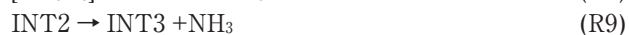


Figure 3 shows the potential energy profiles for these reactions, including the optimized structures of the TSs. Here, HNO₃ aids R9 by decreasing the energy barrier. The rate coefficients for the reactions were evaluated by simple TST and are listed in Table 1. The entire bimolecular reaction can be reduced to one equation: CN₃H₅ → HNCNH + NH₃, adding both sides of R7 to R10.



3.2.2 CN₃H₅ + radicals

A molecule of guanidine is attacked by radicals (OH[•], NO₂[•], and HNCN[•]). This work investigated the reactions

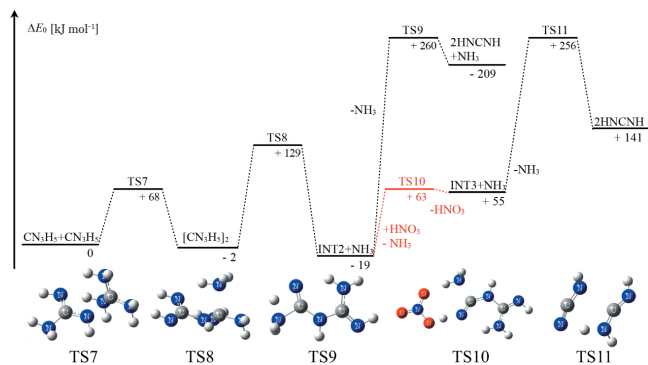


Figure 3 Potential energy profiles for the bimolecular decomposition of guanidine. The energy profiles were calculated at the CBS-QB3// ω B97X-D/6-311++G(d,p) level of theory.

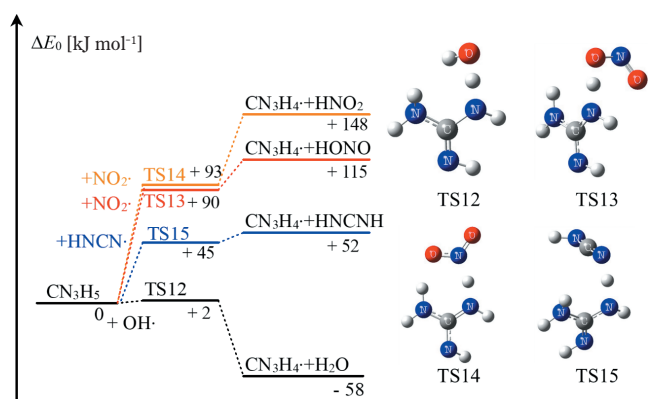


Figure 4 Potential energy profiles for the CN_3H_5 + radicals. The energy profiles were calculated at the CBS-QB3// ω B97X-D/6-311++G(d,p) level of theory.

between CN_3H_5 and the radicals as the following.

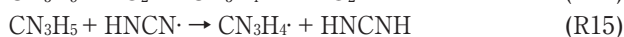


Figure 4 shows the potential energy profiles for the series of reactions, including the optimized structures of the TSs. The rate coefficients for the reactions were evaluated by simple TST and are listed in Table 1.

3.2.3 $\text{CN}_3\text{H}_4\cdot$ decomposition

After generating guanidine radical ($\text{CN}_3\text{H}_4\cdot$) from the CN_3H_5 + radical reaction, $\text{CN}_3\text{H}_4\cdot$ decomposes via intramolecular hydrogen transfer, similar to CN_3H_5 . The decomposition is also aided by some species (M).

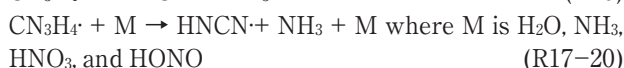


Figure 5 shows the potential energy profiles for the series of reactions, including the optimized structures of the TSs. The rate coefficients for the reactions were evaluated by simple TST and are listed in Table 1.

3.2.4 $\text{CN}_3\text{H}_4\cdot$ + $\text{NO}_2\cdot$ recombination

This work identified the radical recombination between CN_3H_4 and $\text{NO}_2\cdot$, and subsequent reactions as below.

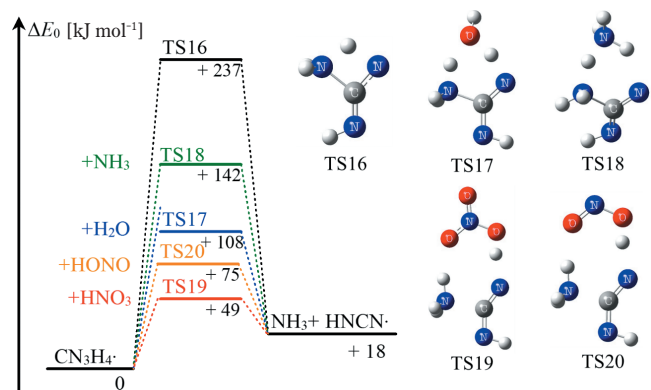


Figure 5 Potential energy profiles for the CN_3H_4 decompositions. The energy profiles were calculated at the CBS-QB3// ω B97X-D/6-311++G(d,p) level of theory.

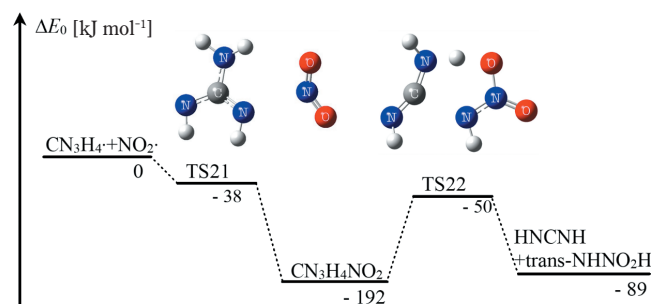


Figure 6 Potential energy profiles for the CN_3H_5 + NO_2 and the followed reaction. The energy profiles were calculated at the CBS-QB3// ω B97X-D/6-311++G(d,p) level of theory.

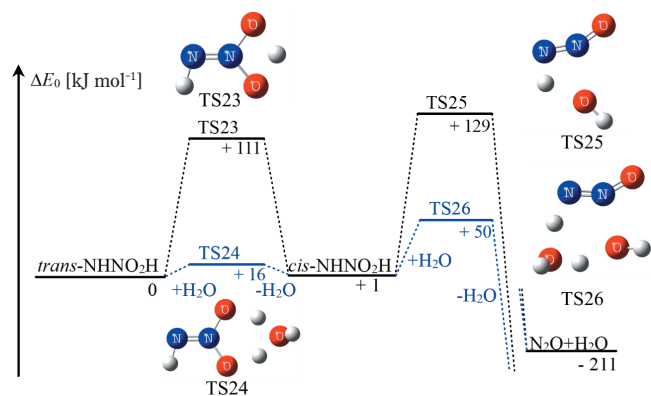


Figure 7 Potential energy profiles for the NHNO_2H decomposition. The energy profiles were calculated at the CBS-QB3// ω B97X-D/6-311++G(d,p) level of theory.

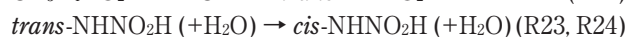
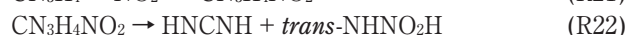


Figure 6 and Figure 7 show schematic potential energy diagrams of these reactions. Here, in the NHNO_2H decomposition, water functions as a catalyst to assist the intramolecular hydrogen transfer (R24 and R26). The rate coefficients for the reactions were evaluated by simple TST.

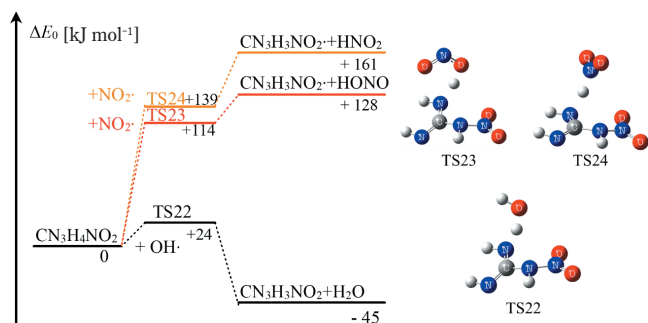


Figure 8 Potential energy profiles for the $\text{CN}_3\text{H}_4\text{NO}_2$ + radicals. The energy profiles were calculated at the CBS-QB3// ω B97X-D/6-311++G(d,p) level of theory.

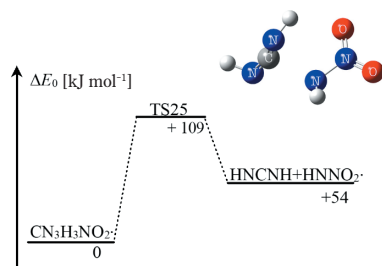


Figure 9 Potential energy profiles for the $\text{CN}_3\text{H}_3\text{NO}_2$ decomposition. The energy profiles were calculated at the CBS-QB3// ω B97X-D/6-311++G(d,p) level of theory.

3.2.5 $\text{CN}_3\text{H}_4\text{NO}_2$ + radicals

$\text{CN}_3\text{H}_4\text{NO}_2$ can also be attacked by radicals (M) as shown below.

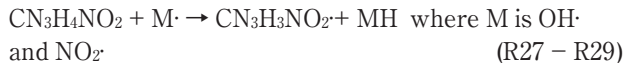


Figure 8 shows the potential energy profiles for the radical reactions, including the optimized structures of the TSs. After the reactions, the generated $\text{CN}_3\text{H}_3\text{NO}_2$ decomposes to HNCNH and HNNO_2 . Figure 9 shows the potential energy profile for the decomposition. The rate coefficients for the reactions were also evaluated by TST.

3.2.6 Other reactions

As discussed above, HNCNH and HNCN \cdot are the major products from CN_3H_5 decomposition. This work investigated and modeled the reactions associated with these species. HNCNH can polymerize to produce melamine, melem, melon, etc. In this study, polymerization is not considered, because HNCNH decomposition proceeds in a flame at high temperature and such conditions promote decomposition over polymerization. First, we investigated the radical reactions as shown below.

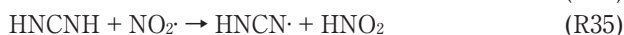
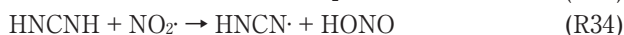


Figure 10 shows the potential energy profiles for the series of reactions, including the optimized structures of the TSs.

Next, this work identified the radical recombination

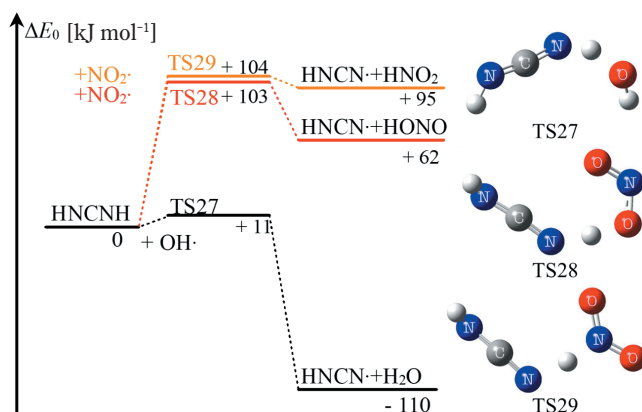


Figure 10 Potential energy profiles for the HNCNH + radicals. The energy profiles were calculated at the CBS-QB3// ω B97X-D/6-311++G(d,p) level of theory.

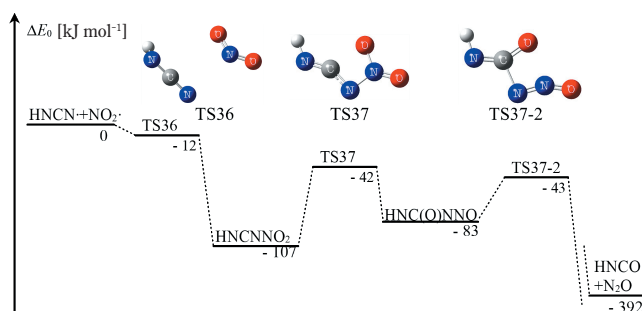


Figure 11 Potential energy profiles for the HNCN \cdot + $\text{NO}_2\cdot$ and followed reactions. The energy profiles were calculated at the CBS-QB3// ω B97X-D/6-311++G(d,p) level of theory.

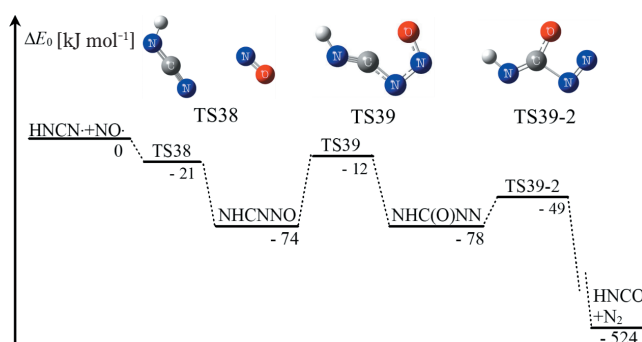
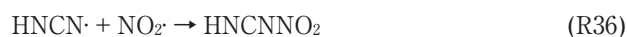


Figure 12 Potential energy profiles for the HNCN \cdot + $\text{NO}\cdot$ and followed reactions. The energy profiles were calculated at the CBS-QB3// ω B97X-D/6-311++G(d,p) level of theory.

according to the following reactions.



Figures 11 and 12 show the potential energy profiles for the series of reactions, including the optimized structures of the TSs. The rate coefficients for the reactions were evaluated by simple TST and are listed in Table 1. The rate coefficients for R36 and R38 were also evaluated by simple TST. On the pathway from R37 to R39, there are two transition states. The energy barrier of the second reaction (TS37-2 and TS39-2) is smaller than that of the first one. The rate coefficient for the reactions was

evaluated by simple TST for TS37 and TS39 by neglecting the intermediate reaction (TS37-2 and TS39-2).

3.3 Simulations

To gain better understanding of the combustion mechanism of GN composition, the YNU 3.0 model was used to calculate the flame structure of a $\text{CH}_5\text{N}_3/\text{HNO}_3/\text{NO}_2/\text{H}_2\text{O}/\text{O}_2 = 9/9/4/6/3$ mol ratio gas mixture at $P_0 = 3$ MPa and $T_0 = 1173$ K in the premixed burner combustion. We simulated the flame structure of GN/BCN with a composition of 9:4 mol ratio (approximately 53:47 mass ratio), which leads to an initial composition of $\text{CH}_5\text{N}_3/\text{HNO}_3/\text{NO}_2/\text{H}_2\text{O} = 9/9/4/6/3$ mol ratio. The initial composition was designed to simulate evolved gas from the burning surface of GN/BCN, which is widely used as a car-airbag propellant. The mixing molar ratio was 9:4 in accordance with the chemical formula for complete combustion following; $9\text{GN} + 4\text{BCN} \rightarrow 9\text{CO}_2 + 20\text{N}_2 + 33\text{H}_2\text{O} + 9\text{Cu}^{26}$. Unfortunately, the precise evolved-gas composition is unknown. In this study, we assumed that following reactions occurs on the burning surface; $\text{GN} (\text{L}) \rightarrow \text{HNO}_3 (\text{G}) + \text{CN}_3\text{H}_5 (\text{G})$ and $2\text{Cu}_2(\text{OH})_3(\text{NO}_3) (\text{S}) \rightarrow \text{Cu}_2\text{O} (\text{L}) + 2\text{NO}_2 (\text{G}) + 3\text{H}_2\text{O} (\text{L}) + \text{O}_2 (\text{G})$. Wada *et al.*²⁷ reported Cu_2O generated from BCN on the burning surface of ammonium nitrate/GN/BCN mixtures similar to GN/BCN. Here, we assumed that the Cu_2O remains on burning surface because of its high boiling temperature (approximately 2073 K). Reactions associated with copper metal and copper oxide was not included in the model. In the future work, effects of metal and metal oxide should be concerned to get full understand of the burning behavior of GN/BCN mixture. The initial gas temperature, i.e., the temperature of the burning surface, is also unknown. We set an initial temperature of 1173 K based on the burning surface temperature of ammonium nitrate/GN/BCN mixtures from the work of Wada *et al.*²⁷ The initial mass flow rate was set at 9.7 g cm^{-3} , calculated from the linear burning rate equation of GN/BCN in the work of Nakashima *et al.*²⁶ We used the CHEMKIN-PRO program suite²⁸ for the calculations.

Temperature and species distance profiles at the initial temperature of $T_0 = 1173$ K are shown in Figure 13. The flame structure of GN-based propellant can be divided into four zones: the first ignition (approximately 0 – 0.005 cm in Figure 13 (A)), the first flame (approximately 0.005 – 0.125 cm), the second ignition (approximately 0.125 – 0.135 cm), and the second flame ($>$ approximately 0.135 cm). In the first ignition zone (Figure 13 (C)), HNO_3 completely decomposes and its mole fraction decreases to almost zero. The mole fraction of CH_5N_3 also decreases to less than half of its initial value. At the same time, N_2O , NO_2 , NO , HNCNH , and H_2O evolve. In the first flame (Figure 13 (B)), the remaining CH_5N_3 and NO_2 are gradually reduced. At the same time, NH_3 and HNCNH increase, and N_2O and NO also slightly increase. In the second ignition, the mole fractions of N_2O and HNCNH sharply decrease to near zero and N_2 , CO , and CO_2 are produced as the temperature skyrockets. The second flame decomposes NO with thermal elevation. Unfortunately, there are no

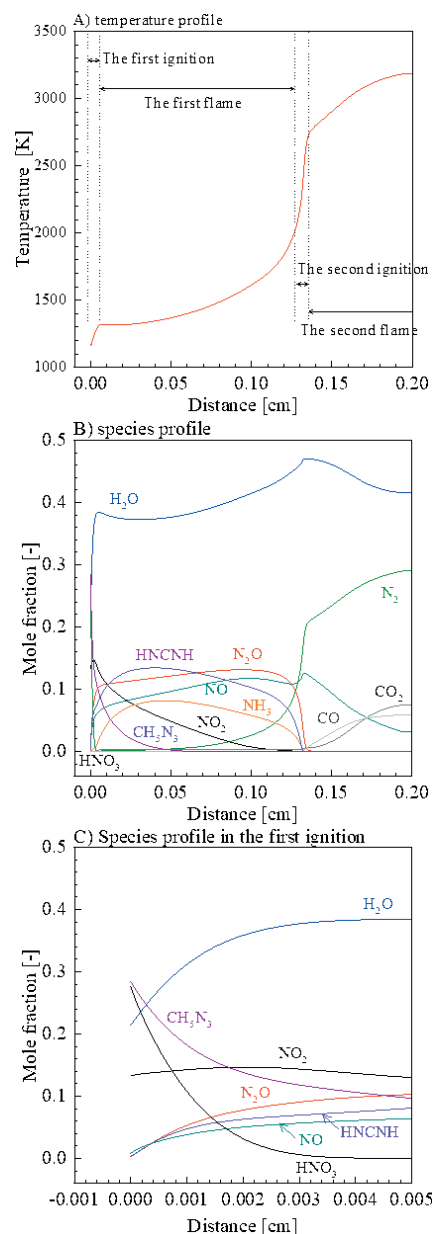


Figure 13 Distance profiles for temperature and important species, calculated based on YNU 3.0 model by CHEMKIN-PRO.

experimental data for the flame structure of the GN/BCN mixture so we cannot directly compare our computational results with experimental data. Further experimental examinations for flame temperature and evolved gases are needed to validate the new model.

To gain a better understanding of the chemical reactions occurring in the flame, we conducted rate of production analysis. Figure 14 shows absolute rates of important species (HNO_3 , CN_3H_5 , CN_3H_4 , and HNCNH) produced in the first ignition and flame zone. In the first ignition zone (approximately 0 – 0.005 cm), HNO_3 decomposes to OH and NO_2 (Figure 14 (A)). The OH radical attacks CN_3H_5 to yield CN_3H_4 (Figure 14 (B)) and the CN_3H_4 combines with NO_2 to form $\text{CN}_3\text{H}_4\text{NO}_2$ (Figure 14 (C)). $\text{CN}_3\text{H}_4\text{NO}_2$ decomposes to yield HNCNH and *trans*- NHNO_2H (Figure 14 (D)). The *trans*- NHNO_2H decomposes into N_2O and H_2O via intramolecular hydrogen transfer.

Figure 15 shows absolute rates of important species

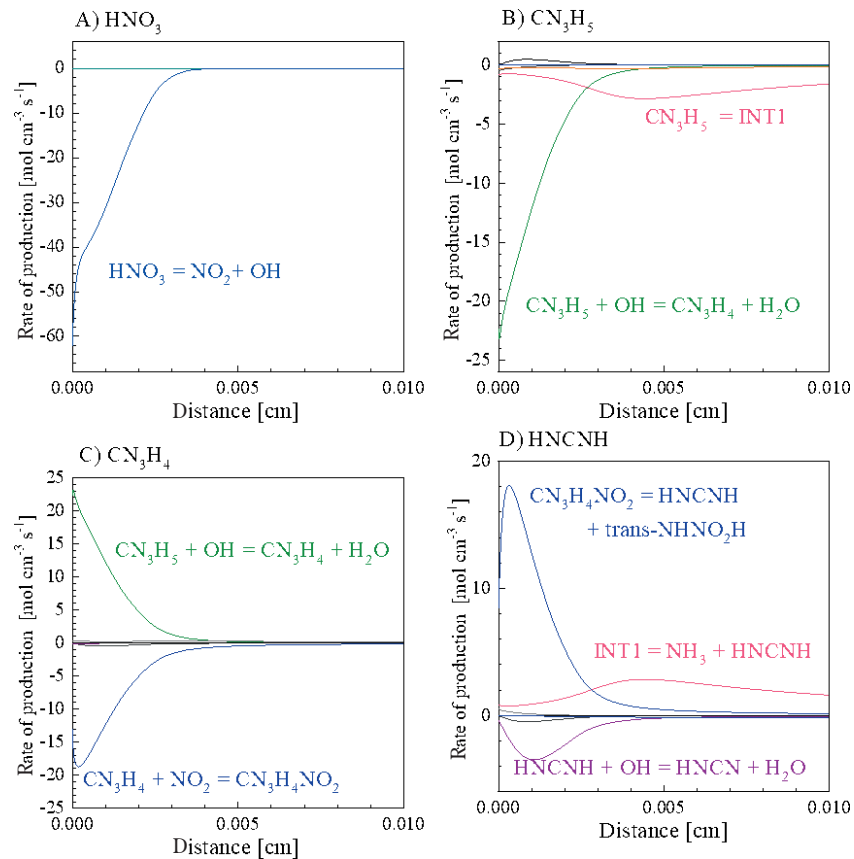


Figure 14 Distance profiles for absolute rate of important species (HNO₃, CN₃H₅, CN₃H₄, and HNCNH) production in the first ignition, calculated based on YNU 3.0 model by CHEMKIN-PRO.

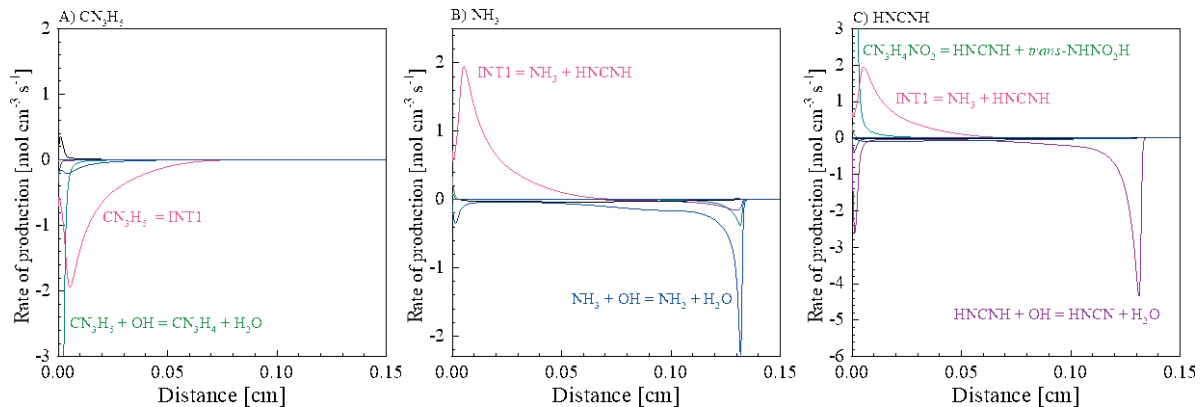


Figure 15 Distance profiles for absolute rate of important species (CN₃H₅, NH₃, and HNCNH) production in the first flame and the second ignition, calculated based on YNU 3.0 model by CHEMKIN-PRO.

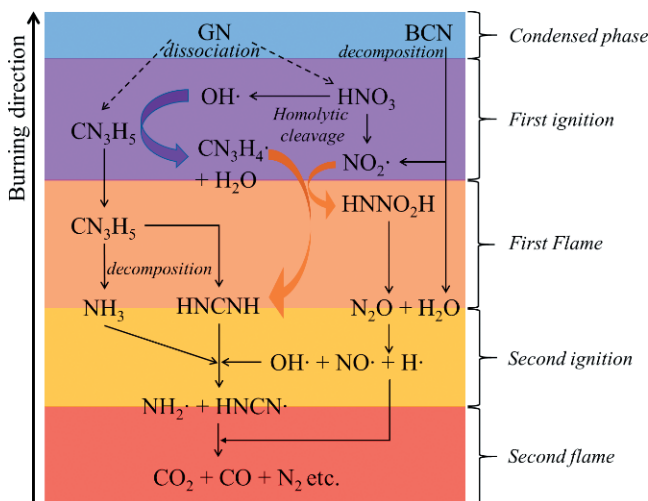


Figure 16 A reaction scheme in flame of GN/BCN mixture.

(CN₃H₅, NH₃ and HNCNH) produced from the first flame to the second ignition. In the first flame following the ignition, remaining CH₅N₃ is consumed by self-decomposition: CH₅N₃ → NH₃ + HNCNH via INT1 (Figure 15 (A)) and the temperature gradually increases. At the end of this area, CH₅N₃ is completely consumed. In the second ignition area (approximately 0.125 – 0.135 cm), combustion and decomposition of HNCNH and NH₃ start with OH· radical attack (Figure 15 (B) and (C)). Figure 16 shows the schematic combustion mechanism of GN/BCN generated from this study.

4. Conclusions

The combustion reactions of guanidine nitrate (GN) in the gas phase were investigated based on quantum chemistry calculations. These calculations were performed

at the ω B97X-D/6-311++G(d,p) and CBS-QB3// ω B97X-D/6-311++G(d,p) levels of theory. Based on the calculations, we modeled various reaction kinetics and developed the new YNU 3.0 model. The new model includes guanidine decomposition, bimolecular reactions between guanidine and radicals, and decompositions of intermediates. The model was created to calculate the flame structure of a $\text{CH}_5\text{N}_3/\text{HNO}_3/\text{NO}_2/\text{H}_2\text{O}/\text{O}_2 = 9/9/4/6/3$ mol ratio gas mixture at $P_0 = 3$ MPa and $T_0 = 1173$ K in the premixed burner combustion. The flame structure of GN-based propellant can be divided into four zones: the first ignition, the first flame, the second ignition, and the second flame. The rate of production analysis reveals the combustion reaction mechanism. In the first ignition area, HNO_3 decomposes to $\text{OH}\cdot$ and NO_2 . The $\text{OH}\cdot$ radical attacks CN_3H_5 to yield CN_3H_4 , which combines with NO_2 to form $\text{CN}_3\text{H}_4\text{NO}_2$. $\text{CN}_3\text{H}_4\text{NO}_2$ decomposes to HNCNH and *trans*- NHNO_2H . The *trans*- NHNO_2H is converted into N_2O and H_2O via intramolecular hydrogen transfer. In the first flame, remaining CH_5N_3 is consumed by self-decomposition: $\text{CH}_5\text{N}_3 \rightarrow \text{NH}_3 + \text{HNCNH}$. In the second ignition area, decomposition of HNCNH and NH_3 starts with $\text{OH}\cdot$ radical attack. Finally, in the second flame, N_2 , CO_2 , and CO are evolved.

Acknowledgement

This research was supported by the Foundation for the Promotion of Industrial Explosives Technology 2017 and JSPS KAKENHI Grant Number 17H00844.

References

- J. W. Schoppelrei, M. L. Kieke, X. Wang, M. T. Klein, and T. B. Brill, *J. Phys. Chem.*, **100**, 14343-14351 (1996).
- M. R. Udupa, *Thermochemica Acta*, **53**, 383-385 (1982).
- Y. I. Rubtsov, A. I. Kazakov, D. B. Lempert, and G. B. Manelis, *Russ. J. Appl. Chem.*, **77**, 1083-1091 (2004).
- R.S. Damse, *J. Hazard. Mater.*, **172**, 1383-1387 (2009).
- J. C. Oxley, J. L. Smith, E. Rogers, W. Naik, and J. Moran, *J. Energ. Mater.*, **27**, 17-39 (2008).
- S. Yoshino and A. Miyake, *J. Therm. Anal. Calorim.*, **102**, 513-516 (2010).
- X. Mei, Y. Cheng, Y. Li, X. Zhu, S. Yan, and X. Li, *J. Therm. Anal. Calorim.*, **114**, 131-135 (2013).
- A. Ulas, G. A. Risha, and K. K. Kuo, *Fuel*, **85**, 1979-1986 (2006).
- P. Thakre, Y. Duan, and V. Yang, *Combust. Flame*, **161**, 347-362 (2014).
- J. Park and M. C. Lin, *J. Phys. Chem. A*, **113**, 13556-13561 (2009).
- J. Park, D. Chacrabarty, and M. C. Lin, *Symp. (Int.) on Combust.*, **27**, 2351-2357 (1998).
- Y. Daimon, H. Terashima, and M. Koshi, *J. Propul. Power*, **30**, 707-716 (2014).
- N. E. Ermolin, *Combust. Explos. Shock Waves*, **40**, 92-109 (2004).
- N. E. Ermolin, *Combust. Explos. Shock Waves*, **43**, 549-561 (2007).
- Y. Izato, M. Koshi, and A. Miyake, *Sci. Tech. Energetic Materials*, **78**, 12-18 (2017).
- Y. Izato and A. Miyake, *Sci. Tech. Energetic Materials*, (2018). (In press).
- J. D. Chai and M. Head-Gordon, *Phys. Chem. Chem. Phys.*, **10**, 6615-6620 (2008).
- M. J. Frisch, G. W. Trucks, H. B. Schlegel, G. E. Scuseria, M. A. Robb, J. R. Cheeseman, G. Scalmani, V. Barone, B. Mennucci, G. A. Petersson, H. Nakatsuji, M. Caricato, X. Li, H. P. Hratchian, A. F. Izmaylov, J. Bloino, G. Zheng, J. L. Sonnenberg, M. Hada, M. Ehara, K. Toyota, R. Fukuda, J. Hasegawa, M. Ishida, T. Nakajima, Y. Honda, O. Kitao, H. Nakai, T. Vreven, J. A. Montgomery, J. E. Peralta, F. Ogliaro, M. Bearpark, J. J. Heyd, E. Brothers, K. N. Kudin, V. N. Staroverov, T. Keith, R. Kobayashi, J. Normand, K. Raghavachari, A. Rendell, J. C. Burant, S. S. Iyengar, J. Tomasi, M. Cossi, N. Rega, J. M. Millam, M. Klene, J. E. Knox, J. B. Cross, V. Bakken, C. Adamo, J. Jaramillo, R. Gomperts, R. E. Stratmann, O. Yazyev, A. J. Austin, R. Cammi, C. Pomelli, J. W. Ochterski, R. L. Martin, K. Morokuma, V. G. Zakrzewski, G. A. Voth, P. Salvador, J. J. Dannenberg, S. Dapprich, A. D. Daniels, O. Farkas, J. B. Foresman, J. V. Ortiz, J. Cioslowski, and D. J. Fox, *Gaussian 09*, Revision D.01, Gaussian, Inc., Wallingford CT (2010).
- J. A. Montgomery, M. J. Frisch, J. W. Ochterski, and G. A. Petersson, *J. Chem. Phys.*, **110**, 2822-2827 (1999).
- A. Matsugi and H. Shiina, *Bull. Chem. Soc. Jpn.*, **87**, 890-901 (2014).
- A. Miyoshi, GPOP software, rev. 2013.07.15 m5, available from the author. See <http://akrmys.com/index.html> (accessed: 14-June-2018). (online).
- L. A. Curtiss, P. C. Redfern, and K. Raghavachari, *J. Chem. Phys.*, **126**, 084108 (2007).
- A. Nikolaidis, A. Rauk, M. N. Glukhovtsev, and L. Radom, *J. Phys. Chem.*, **100**, 17460-17564 (1996).
- R. J. Kee, F. M. Rupley, and J. A. Miller, "The Chemkin Thermodynamic Data Base", Sandia National Laboratories Report, SAND87-8215B (1990).
- A. Burcat and B. Ruscic, "Third Millennium Ideal Gas and Condensed Phase Thermochemical Database for Combustion with Updates from Active Thermochemical Tables", ANL-05/20, TAE960 (2005).
- M. Nakashima, T. Itaura, H. Matsunaga, E. Higashi, S. Takagi, and K. Katoh, *J. Therm. Anal. Calorim.*, **131**, 95-100 (2018).
- Y. Wada, K. Hori, and M. Arai, *Sci. Tech. Energetic Materials*, **71**, 83-87 (2010).
- CHEMKIN-Pro Input Manual PRO-INP-15092-UG-1, Reaction Design, San Diego, CA (2011).